Effects of bound states on dark matter annihilation

Haipeng An,* Mark B. Wise,† and Yue Zhang‡
Walter Burke Institute for Theoretical Physics, California Institute of Technology, Pasadena, California 91125, USA
(Received 14 April 2016; published 15 June 2016)

We study the impact of bound state formation on dark matter annihilation rates in models where dark matter interacts via a light mediator, the dark photon. We derive the general cross section for radiative capture into all possible bound states, and point out its nontrivial dependence on the dark matter velocity and the dark photon mass. For indirect detection, our result shows that dark matter annihilation inside bound states can play an important role in enhancing signal rates over the rate for direct dark matter annihilation with Sommerfeld enhancement. The effects are strongest for large dark gauge coupling and when the dark photon mass is smaller than the typical momentum of dark matter in the Galaxy. As an example, we show that for thermal dark matter the Fermi gamma ray constraint is substantially increased once bound state effects are taken into account. We also find that bound state effects are not important for dark matter annihilation during the freeze-out and recombination epochs.

DOI: 10.1103/PhysRevD.93.115020

I. INTRODUCTION

It is very likely that dark matter (DM) requires degrees of freedom that are not in the standard model (SM) for its explanation. As its name implies the electromagnetic interactions of DM must be small. A convenient way to realize this is to suppose that the DM is not charged under the SM gauge group. A simple model of this type that does not have any fine tunings, beyond the usual ones to keep the cosmological constant and Higgs mass small, is to have the DM be a Dirac fermion coupled to a new massive $U(1)_D$ gauge boson (the dark photon). Since the DM couples to a conserved current the new gauge boson can have a mass term in the Lagrange density. This model adds to the SM seven new dark degrees of freedom: two spin components for both the DM and anti-DM particles, and the three spin states for the massive dark photon. The model has three additional parameters, a dark fine structure constant, $\alpha_D = g_D^2/(4\pi)$, the DM mass m_D and the dark photon mass m_V. In addition there is one dimensionless renormalizable coupling κ that characterizes the kinetic mixing of the hypercharge $U(1)_Y$ and $U(1)_D$ kinetic terms. It is only through gravity and this kinetic mixing that SM degrees of freedom communicate with those in the dark sector.

In this paper we will assume thermal DM, i.e., at early times when the Universe is at a very high temperature, the DM sector is in thermal equilibrium, and moreover has the same temperature as the SM. As the Universe evolves it cools and when the temperature drops below the DM mass, DM and anti-DM particles start to annihilate, eventually freezing out at $T \sim m_D/30$. In this scenario achieving the correct DM density relates the dark fine structure constant to the DM mass, roughly $\alpha_D \sim 0.02(m_D/1\ \text{TeV})$. For DM much heavier than a TeV, one needs to take into account the Sommerfeld effect during freeze-out and α_D is somewhat lower than the value predicted by the above relation. For example, $\alpha_D = 0.2$ for $m_D = 16.7$ TeV.

The light mediator scenario with $m_D \gg m_V$ has been studied for a variety of reasons. In the same region of parameter space there are indirect detection signals that are the topic of study in this paper. For $\alpha_D m_D/(2m_V) > 0.84$, two body DM-anti-DM bound states exist. They are the analog of positronium bound states in electromagnetism. It is the impact of these darkonium bound states on the rate for DM-anti-DM annihilation in the Galaxy today that we focus on.

The region of parameter space in the $m_V - m_D$ plane where bound states exist and are potentially important for DM cosmology is shown in Fig. 1. We assume these darkonium states are nonrelativistic and so we restrict our attention to the region of parameter space where $\alpha_D < 0.3$ or its equivalent (for thermal DM $m_D < 30$ TeV). Very small dark photon masses, $m_V < 30$ MeV, are inconsistent with direct detection, the supernova constraints and the requirement that dark photons decay away before big bang nucleosynthesis (BBN). The region of Fig. 1 below the green line does not have darkonium states and the region between the brown and green lines has darkonium states but the mass of the dark photon is too large for these bound states to be produced with the low kinetic energy for the DM during recombination or at the Galactic center. Thus, the region of parameter space for our study of the impact of bound states on indirect detection signals is the triangular region marked as the "Focus of this study" in Fig. 1.

*anhp@caltech.edu
†wise@theory.caltech.edu
‡yuezhang@theory.caltech.edu

The main finding of our work is that the bound state effects are important for DM indirect detection when $m_V/m_D \lesssim 10^{-3}$ and $\alpha_D \gtrsim 0.1$. The goal of this paper is not to provide a comprehensive list of all the indirect detection constraints but rather to highlight the important role bound state formation plays in this region of parameter space. To this end we focus on the photon spectrum resulting from DM near the center of our Galaxy annihilating either directly or through bound states.

In Sec. II, we derive the general cross section for dark matter bound state formation via radiation of an on-shell dark photon and its dependence on the dark matter velocity and the dark photon mass. In Sec. III, we apply our results to calculate the indirect detection constraints on dark matter annihilation and discuss the importance of bound state effects. We discuss the bound state effects on dark matter freeze-out and on the cosmic microwave background (CMB) in Secs. IV and V, and conclude in Sec. VI.

II. BOUND STATE FORMATION CROSS SECTION

The Lagrangian for the dark sector is

$$\mathcal{L} = \mathcal{L}_{\rm SM} + \bar{\chi} i\gamma^\mu(\partial_\mu - i g_D V_\mu)\chi - m_D\bar{\chi}\chi - \frac{1}{4}V_{\mu\nu}V^{\mu\nu} + \frac{1}{2}m_V^2 V_\mu V^\mu - \frac{\kappa}{2\cos\theta_w}B_{\mu\nu}V^{\mu\nu}, \quad (1)$$

where $B_{\mu\nu}$ is the hypercharge field strength tensor and θ_w is the Weinberg angle. Hence κ is the kinetic mixing between the photon and the vector field V.

The interaction Hamiltonian for radiating one dark photon V can be separated into transverse and longitudinal mode parts. In the center-of-mass frame, the Hamiltonian for radiating transverse V's is

$$H_{\rm int}^T = \left(\frac{g_D\mathbf{k}}{\mu}\right)\left[\mathbf{A}_T\left(\frac{\mathbf{r}}{2}\right) + \mathbf{A}_T\left(-\frac{\mathbf{r}}{2}\right)\right], \quad (2)$$

where $\mathbf{r}$ is the relative coordinate of χ and $\bar{\chi}$, $\mathbf{k}$ is the relative DM momentum and $\mu = m_D/2$ is the DM reduced mass. For the transverse modes, the polarization vectors satisfy $\epsilon_i^+(q)\epsilon_j^{+*}(q) + \epsilon_i^-(q)\epsilon_j^{-*}(q) = \delta_{ij} - q_i q_j/|\mathbf{q}|^2$, and $\mathbf{q}$ is the three-momentum of the radiated dark photon. For radiating a longitudinal V, using current conservation $q^\mu J_\mu = 0$, the interaction Hamiltonian can be written as

$$H_{\rm int}^L = \left(\frac{g_D m_V}{|\mathbf{q}|}\right)\left[\phi_L\left(\frac{\mathbf{r}}{2}\right) - \phi_L\left(-\frac{\mathbf{r}}{2}\right)\right]. \quad (3)$$

Effectively it is equivalent to radiating a scalar particle.

For bound state formation, $|\mathbf{q}| \sim \alpha_D^2\mu$ and $|\mathbf{r}| \sim 1/(\alpha_D\mu)$, where $\alpha_D = g_D^2/(4\pi)$. Thus we use the dipole approximation and only keep the leading terms in $\mathbf{q}\cdot\mathbf{r}$. Then the matrix elements for the free-bound transitions with transverse and longitudinal V radiation are

$$\mathcal{M}_T = g_D\int d^3\mathbf{r}\Psi_f^*(\mathbf{r})(E_i - E_f)\mathbf{r}\cdot\epsilon_T\Psi_i(\mathbf{r}),$$
$$\mathcal{M}_L = -ig_D\int d^3\mathbf{r}\Psi_f^*(\mathbf{r})m_V\frac{\mathbf{r}\cdot\mathbf{q}}{|\mathbf{q}|}\Psi_i(\mathbf{r}). \quad (4)$$

The total cross section for bound state formation from a scattering state with momentum $\mathbf{k}$ at infinity is

$$(\sigma v)_{\rm B} = \frac{\alpha_D}{3\pi}\sum_{n,\ell}\left(\omega_{n\ell}^2 + \frac{1}{2}m_V^2\right)\sqrt{\omega_{n\ell}^2 - m_V^2} \times\left[\ell\left|\int dr r^3 R_{n\ell}(r)R_{k\ell-1}\right|^2 + (\ell+1)\left|\int dr r^3 R_{n\ell}(r)R_{k\ell+1}\right|^2\right], \quad (5)$$

where v is the relative velocity and $\omega_{n\ell} = E_{n\ell} + k^2/(2\mu)$ is the sum of the binding energy of the $(n\ell)$th bound state level and the kinetic energy of incoming state. For a

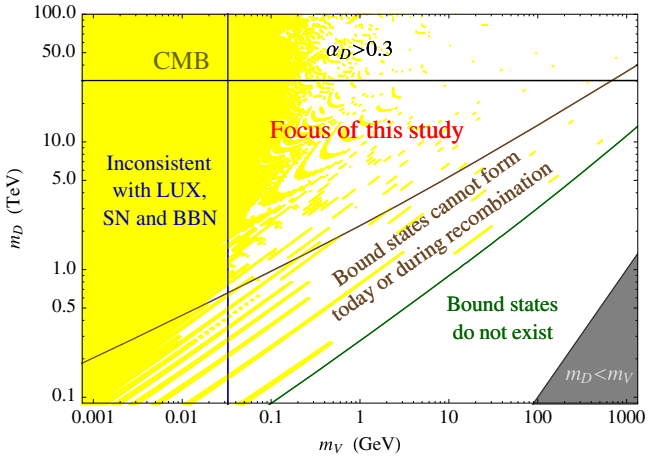

FIG. 1. The parameter space relevant to this study (marked by "Focus of this study"), where m_D is the dark matter mass and m_V is the dark photon mass. The value of the dark fine structure constant $\alpha_D = g_D^2/(4\pi)$ is chosen to give the correct relic abundance for dark matter. We do not consider $\alpha_D < 0.3$ (above the black curve) where the next-to-leading order corrections would be large. The gray region at the lower right corner does not satisfy the light mediator condition, thus we also do not consider it. Dark matter bound states do not exist below the green curve. Between the brown and green curves, dark matter bound states exist but the dark photon is too heavy for the bound states to be produced with the low kinetic energy such as in the Galaxy today or during recombination. The region to the left of the blue curve is excluded by direct detection, the supernova constraints and demanding that dark photons decay before BBN, see also Fig. 4. The yellow region is excluded by CMB constraints on dark matter annihilation during recombination, see Sec. V.

Yukawa potential, the binding energy in general depends on both n and ℓ.

A couple of remarks relevant to the evaluation of Eq. (5) follow.

(i) The sum over n, ℓ includes all the energy levels satisfying $\omega_{n\ell} > m_V$. For low velocity DM with $k^2/(2\mu) \ll m_V$, this amounts to $E_{n\ell} > m_V$. As a rough estimate we can use $E_{n\ell} \sim \alpha_D^2\mu/(2n^2)$ for the binding energy. Then if $E_{n\ell} > m_V$, the ratio of the bound state size to the screening length of the Yukawa potential, $a_n m_V \sim n m_V/(\alpha_D\mu)$, is less than $\alpha_D/(2n) \ll 1$. In other words, those bound states that are deep enough to emit an on-shell V in their formation are all much smaller than $1/m_V$. Therefore, from now on, we will approximate the relevant bound states as Coulomb bound states, with energies $E_{n\ell} = E_n$, $\omega_{n\ell} = \omega_n$, that are ℓ independent.

(ii) The bound and scattering wave functions that solve the Schrödinger equation are written as

$$\psi_n(\mathbf{r}) = \sum_{\ell m} R_{n\ell}(r) Y_{\ell m}(\hat{r}),$$
$$\psi_k(\mathbf{r}) = \sum_{\ell m} R_{k\ell}(r) Y_{\ell m}(\hat{r}) Y^*_{\ell m}(\hat{k}). \quad (6)$$

Using the above approximation, the radial Coulomb wave functions for bound states are

$$R_{n\ell}(r) = \frac{2}{n^{\ell+2}(2\ell+1)!}\sqrt{\frac{(n+\ell)!}{(n-\ell-1)!}}\frac{(2r)^\ell}{a_0^{\ell+3/2}} \times e^{-(r/na_0)} F_1\left(1+\ell-n, 2+2\ell, \frac{2r}{na_0}\right), \quad (7)$$

where $a_0 = 1/(\alpha_D\mu)$ is the Bohr radius.

For the scattering state radial wave functions, we numerically solve the Schrödinger equation with a Yukawa potential and energy eigenvalue $E = k^2/(2\mu)$ using the "shooting method." For the ℓth partial wave, define $R_{k\ell}(r) = r^{\ell-1}\phi(r)$, the Schrödinger equation for $\phi(r)$ is

$$\phi''(r) + \frac{2\ell}{r}\phi'(r) + \left(k^2 + \frac{2\alpha\mu e^{-m_V r}}{r} - \frac{2\ell}{r^2}\right)\phi(r) = 0. \quad (8)$$

The boundary condition at $r = 0$ is $\phi(0) = 0$ and $\phi'(0) = c$. Because Eq. (8) is a linear equation, the overall normalization of R is proportional to the parameter c, and we fix it by requiring that $R_{k\ell}$ matches to the ℓth partial of a plane wave as $r \to \infty$, i.e.,

$$rR_{k\ell}(r\to\infty) \sim \frac{(4\pi)}{k} i^\ell \cos\left(kr - (\ell+1)\frac{\pi}{2} + \delta_{k\ell}\right). \quad (9)$$

In the $m_V \to 0$ limit, $R_{k\ell}$ is given by the Coulomb scattering wave function,

$$R_{k\ell}(r) = \frac{4\pi e^{\frac{\pi}{2ka_0}}\left|\Gamma\left(1+\ell-\frac{i}{ka_0}\right)\right|}{(2\ell+1)!}(2kr)^\ell e^{-ikr}\,{}_1F_1 \times \left(1+\ell+\frac{i}{ka_0}, 2+2\ell, 2ikr\right). \quad (10)$$

We first discuss the m_V dependence of the bound state formation cross section in Eq. (5). In the Coulomb limit $m_V \to 0$, it is the Kramers formula for the recombination cross section [1]. For $\alpha_D \gg k/\mu \equiv v$, the leading terms of the Kramers formula for the cross section are [2]

$$\sigma_B = \frac{32\pi}{3\sqrt{3}}\frac{\alpha_D^3}{\mu^2 v^2}\left[\ln\left(\frac{\alpha_D}{v}\right) + 0.16 + \mathcal{O}(v/\alpha)\right]. \quad (11)$$

The logarithmic factor arises from the sum over n in Eq. (5). For a given level $n \gg 1$ [3],

$$(\sigma_B)_n \simeq \frac{32\pi}{3\sqrt{3}}\frac{\alpha_D}{\mu^2}\frac{E_0^2}{(\mu v^2/2)(\mu v^2/2 + E_0/n^2)n^3}. \quad (12)$$

Recall E_0 is the binding energy of the Coulomb bound state, $E_0 = \alpha_D^2\mu/2$. The condition $\alpha_D > v$ implies $E_0 > \mu v^2/2$. It is important to note that $\sigma_n \sim 1/n$ for a small n and $\sigma_n \sim 1/n^3$ for a large n. The transition between these two behaviors occurs around $n_{\rm trans} \sim \alpha_D/v$. The sum of σ_n from $n = 1$ to $n_{\rm trans}$ results in the logarithmic factor $\ln(\alpha_D/v)$ in Eq. (11).[1]

For $m_V \neq 0$ the situation is more complicated. For nonzero mediator mass m_V, we solved for the cross section numerically using the approach described above. As m_V grows, the first effect it has is to change the upper limit of the sum over n. The largest $n_{\rm max}$ corresponds to the highest energy level that has a large enough binding energy that allows V to be produced on shell. When we are still within

[1]We have verified the Kramers formulas (11) and (12) numerically. The calculations taking into account only the capture into ground state [4–7] would miss the logarithmic factor and underestimate the cross section, for the cases $\alpha_D \gg v$ and/or $\alpha_D \gg \sqrt{m_V/m_D}$. We also note that Refs. [8,9] tried to sum over all the energy levels ($n \geq 1$) but concluded it yields a factor of $\pi^2/6$ compared to the ground state case. However, they used the recombination cross section equation (75.6) in [3] that only applies for $n = 1$ and also underestimated the enhancement. Moreover, these previous works have assumed a massless dark photon limit which would neglect the nontrivial m_V dependence as shown in Fig. 2.

the Coulomb limit, $n_{\max} = \alpha_D \sqrt{\frac{\mu}{2m_V}}$. When $n_{\max} < n_{\text{trans}}$, the Kramers cross section is modified to

$$\sigma_{\text{B}} \simeq \frac{32\pi}{3\sqrt{3}} \frac{\alpha_D^3}{\mu^2 v^2} \ln\left(\alpha_D \sqrt{\frac{\mu}{2m_V}}\right). \tag{13}$$

The condition that $n_{\max} < n_{\text{trans}}$ is equivalent to $\mu v^2/2 < m_V$ and we find numerically that Eq. (13) is valid in the range $\frac{1}{2}\mu v^2 < m_V < \mu v$. In the region $m_V > \mu v$, the cross section is resonantly enhanced when the kinetic energy of the incoming state is nearly degenerate with a resonance state of the Yukawa potential. These features are shown in Fig. 2. In the region $\alpha_D^2 m_D/4 < m_V < \alpha_D^2 m_D/16$ only the ground state is available, which is in s-wave. Therefore, due to the nature of dipole transition, in this region the initial state must be in p-wave, and the single-peak resonances shown in Fig. 2 correspond to p-wave resonances. In a smaller m_V region, more and more bound states become available, one can see multiple-peak resonances.

Next, we discuss the velocity dependence of the bound state formation cross section, and highlight the comparison with the Sommerfeld enhanced cross section of direct annihilation, often used for computing DM annihilation in the literature [4,10–12]. This comparison is shown in Fig. 3 for $m_D = 16.7$ TeV, $\alpha_D = 0.2$ and $m_V = 10$ GeV. We find that in the region $m_V/\mu < v < \sqrt{2m_V/\mu}$ the bound state formation cross section is consistently larger than the direct annihilation cross section with Sommerfeld enhancement (labeled with subscript A). For this range of

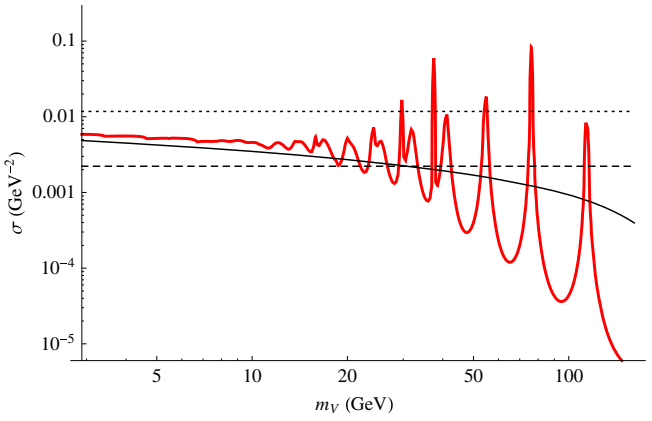

FIG. 2. Dark photon mass dependence in the bound state formation cross section in today's Galaxy (thick red curve), calculated from the general formula, Eq. (5). We have fixed the other parameters to be $m_D = 16.7$ TeV, $\alpha_D = 0.2$ and the velocity $v = 10^{-3}$. The solid black curve is obtained from the modified Kramers formula equation (13), which does not capture the resonance effects. The horizontal dotted line is the original Kramers formula in the Coulomb limit ($m_V \to 0$), Eq. (11), and the dashed line corresponds to only a ground state formation with a massless dark photon with $n = 1$.

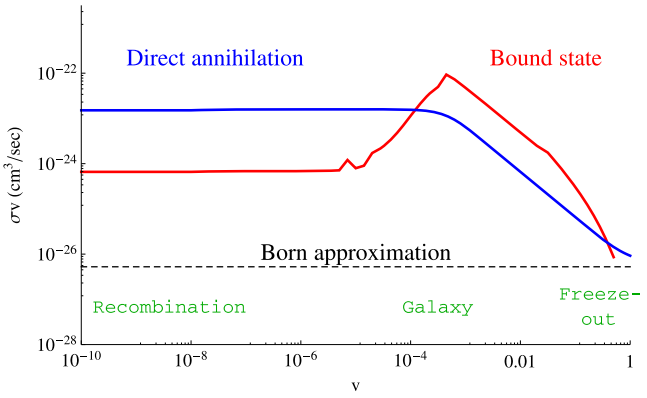

FIG. 3. Dark matter bound state formation cross section for various dark matter velocities (thick red curve), calculated from the general formula, Eq. (5). We have fixed the other parameters, $m_D = 16.7$ TeV, $\alpha_D = 0.2$ and $m_V = 10$ GeV. For comparison, we also show the direct annihilation cross section in the Born approximation (dashed black) and the one with Sommerfeld enhancement (thick blue curve). The bound state formation cross section plays the most important role for dark matter indirect detection if $m_V/m_D < v < \alpha_D$.

relative velocities, the two cross sections can be approximated as

$$(\sigma v)_{\text{B}} \sim \frac{32\pi\alpha_D^3}{3\sqrt{3}\mu^2 v} \ln\left(\alpha_D \sqrt{\frac{\mu}{2m_V}}\right), \qquad (\sigma v)_{\text{A}} \sim \frac{\pi^2 \alpha_D^3}{2\mu^2 v}. \tag{14}$$

The direct annihilation cross section $(\sigma v)_{\text{A}}$ is obtained by enhancing the Born level cross section by the s-wave Sommerfeld factor, defined as $|R_{k,\ell=0}|^2/(4\pi)^2$ in our convention.

The ratio of the two above cross sections is

$$\frac{\text{Bound state formation rate}}{\text{Direct Annihilation rate}} = \frac{(\sigma v)_{\text{B}}}{(\sigma v)_{\text{A}}} = \frac{64}{3\sqrt{3\pi}} \ln\left(\alpha_D \sqrt{\frac{\mu}{2m_V}}\right). \tag{15}$$

With the parameters used in Fig. 3, the bound state formation cross section can be larger by more than one order of magnitude over the Sommerfeld enhanced annihilation cross section.

For $v > \sqrt{2m_V/\mu}$, the bound state production cross section is given by the Kramers formula in Eq. (11) and the logarithmic enhancement factor is suppressed compared with the region of velocity we have just discussed. This is the region to the right in Fig. 3. Eventually, at $v \sim \alpha_D$, the argument of the log factor is ~ 1 and the Kramers and Sommerfeld cross sections become comparable to each other.

For $v < m_V/\mu$, the kinetic energy of the incoming state $\frac{1}{2}\mu v^2$ becomes smaller than the height of the bump of the Yukawa potential barrier $V_{\rm barrier} \sim \ell(\ell+1)m_V^2/\mu$ for the $\ell \neq 0$ partial wave, located near $r \sim 1/m_V$. As v decreases, it becomes increasingly more difficult for these partial wave states to penetrate through the barrier to find the bound state wave function. In this region, the contributions to the bound state formation cross section from all partial waves with $l \neq 0$ are suppressed. Eventually, at a very tiny v, only the $ks \to np, (n \geq 2)$ transitions can happen. In this region the bound state formation cross section is smaller than the Sommerfeld enhanced annihilation cross section.

The above velocity dependence can have an important impact on indirect detection of DM annihilation in the Milky Way Galaxy, where the DM velocity is $\sim 10^{-3}$. We find for $m_V/\mu < 10^{-3}$ and $\alpha_D > 0.1$ (corresponding to multi-TeV scale thermal DM), it is much more likely for two DM particles to form a bound state than to directly annihilate.

After a bound state is formed, it could either annihilate decaying to dark photon V's or deexcite to a lower state. The annihilation decay rate for the $n\ell$ bound state goes as

$$\Gamma_{n,s,\ell\to V's} \sim \left(\frac{\alpha_D}{n}\right)^{2\ell+3} \alpha_D^{(5-C)/2}\mu, \tag{16}$$

where $s = 0, 1$ is the total spin angular momentum of the bound state, n is the principal quantum number, ℓ is the orbital angular momentum and $C = (-1)^{\ell+S}$ is the charge conjugation. For $C = 1$, the bound state decays into $2V$'s, while for $C = -1$, it decays into $3V$'s due to Furry's theorem in the dark sector. The ℓ dependence arises because the annihilation decay amplitude is proportional to the ℓth derivative of the zero point wave function at the origin, $(d^\ell/dr^\ell)R_{n\ell}(0)$. Each derivative yields a power of α_D. For a smaller n (and hence ℓ) the time scale for darkonium annihilation to dark gauge bosons is extremely short compared with the age of our Galaxy, which in units of inverse GeV is $\tau_g \sim 0.62 \times 10^{42}$ GeV^{-1}. But for larger principal quantum numbers n and values of ℓ that is not the case. As an explicit example, we consider the parameters $m_D = 16.7$ TeV, $\alpha_D = 0.2$ and $m_V = 1$ GeV. For these parameters $n_{\rm max} = 12$ and for this value of the principal quantum number, $\ell = n_{\rm max} - 1 = 11$ and $C = -1$, the bound state annihilation decay has a lifetime associated with it that is about one order of magnitude larger than the age of our Galaxy.

Darkonium states with a larger n and ℓ produced in our Galaxy do disappear but the route is through deexcitation to lower values of n and ℓ and then annihilation to energetic V's with $E_V \simeq m_D/2$. For simplicity we consider the case where the transition is dark electric dipole to either a real or, if that is kinematically not allowed, a virtual V. When this can occur via a real dark V the rate is very rapid. For

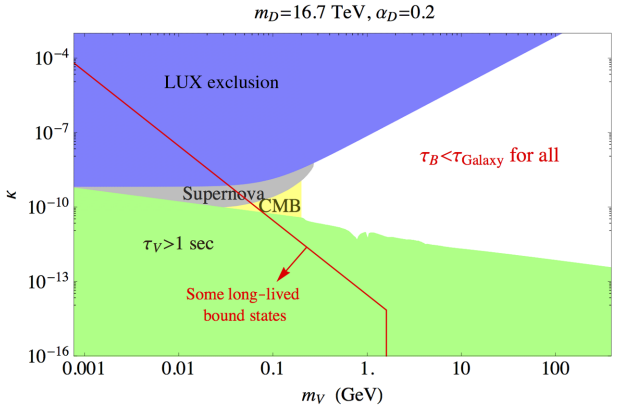

FIG. 4. Constraints on the $m_V - \kappa$ parameter space for fixed $m_D = 16.7$ TeV and $\alpha_D = 0.2$. The blue region is excluded by the LUX result in dark matter direct detection [13]. The gray region is excluded from the supernova cooling argument [14–16]. In the green region, the dark photon lives longer than a second and would threaten the success of BBN assuming the dark and SM sectors had similar temperatures [17,18]. In the allowed (white) region, all possible dark matter bound states have lifetimes shorter than the age of the Milky Way Galaxy.

deexcitation through a virtual V we estimate the rate for the bound state transition $n, \ell \to n-1, \ell \pm 1$ to be

$$\Gamma_{n\to n-1} \sim \frac{\kappa^2\alpha\alpha_D^{13}}{n^{19}}\frac{\mu^5}{4\pi^2 m_V^4}. \tag{17}$$

It is convenient to introduce the "partial lifetimes," $\tau_{n\to n-1} = 1/\Gamma_{n\to n-1}$. Assuming the transition to the ground state occurs changing n by one unit at a time the total rate is

$$\Gamma_{n\to 1} \sim \left(1\Big/\sum_{i=2}^{n}\tau_{i\to i-1}\right) \sim 20\frac{\kappa^2\alpha\alpha_D^{13}}{n^{20}}\frac{\mu^5}{4\pi^2 m_V^4}. \tag{18}$$

We find in this case for the allowed values of κ, m_D and m_V that this deexcitation rate is shorter than the age of the Galaxy. This is illustrated in Fig. 4 using the same parameters as before (i.e., $m_D = 16.7$ TeV, $\alpha_D = 0.2$, $m_V = 1$ GeV and $n_{\rm max} = 12$). All the darkonium bound states produced in our Galaxy do decay converting eventually into two or three very energetic V's and some softer V's which all decay to standard model particles.

Without loss of generality, we imagine there is just one type of bound state. Then its number density n_B satisfies the rate equation

$$\frac{dn_B}{dt} = -\Gamma_B n_B + \frac{1}{4}n_D^2\langle\sigma v\rangle_{\rm B}, \tag{19}$$

where n_D is the unbound DM particle density,[2] Γ_B is the decay rate of the dark bound state and $\langle\sigma v\rangle_{\rm B}$ is the DM

[2] n_D is the sum of DM and anti-DM particle number densities.

bound state production cross section multiplied by the relative velocity of the DM particles. In the Galaxy, if only a small fraction of DM has formed bound states or annihilated today, the free DM density n_D is constant in time. Solving the rate equation for the number density of dark bound states using this approximation gives

$$n_B(t) = \frac{1}{4\Gamma_B} n_D^2 (\sigma v)_{\rm B} (1 - e^{-\Gamma_B t}). \tag{20}$$

Taking the time t to be the age of our Galaxy, $\tau_g \sim 10^{18}$ sec, for $\Gamma_B t \gg 1$, the value of n_B approaches an equilibrium value given by $4 n_B \Gamma_B = n_D (\sigma v)_{\rm B}$.

The DM today includes both free DM and that inside (unstable) bound states $n_D^{(\rm tot)} = n_D + 2 n_B$. The total annihilation rate R relevant to the indirect detection signal, including DM annihilation both directly [$\propto (\sigma v)_A$] and inside the bound states [$\propto (\sigma v)_B$], is

$$R = 2 n_B \Gamma_B + \frac{1}{2} n_D^2 (\sigma v)_{\rm A} = \frac{1}{2} n_D^2 [(\sigma v)_{\rm A} + (\sigma v)_{\rm B}], \tag{21}$$

where, in the second step, we have used the above equilibrium value for n_B. Hence the indirect detection signal discussed in the next section is fully determined by the sum of DM direct annihilation and bound state formation rates.

III. INDIRECT DETECTION

In this section, we quantify the importance of bound state formation on DM indirect detection. The V particles from the annihilation of DM will further decay into SM charged particles via the kinetic mixing with the photon and the Z boson, and contribute to the cosmic gamma ray spectrum. We will consider the Fermi constraint on the photon spectrum from DM annihilation at the Galactic center [19]. The goal of this paper is not to provide a comprehensive list of all the constraints but rather to highlight the important role bound state formation plays in some regions of parameter space.

The gamma ray flux at Earth is obtained from the DM annihilation rate averaged over the Galactic center region via

$$\frac{d\Phi_\gamma}{dE_\gamma} = \sum_{n=2}^{3} \frac{1}{16\pi m_D^2} \frac{dN_\gamma^{(n)}}{dE_\gamma} \int d\Omega \int_{\rm l.o.s.} ds \rho(r(s,\theta))^2 (\sigma v)_{nV}, \tag{22}$$

where ρ is the DM density profile, s is the distance of the annihilation point to Earth, θ is the angle between the line of sight and the direction of the Galactic center in view of Earth, $r(s,\theta) = \sqrt{r_\odot^2 + s^2 - 2 r_\odot s \cos\theta}$ and $r_\odot = 8.4$ kpc is the distance between Earth (or the Sun) and the Galactic center. We use the Navarro-Frenk-White profile for dark matter mass density distribution in the Galaxy,

$$\rho(r) = \frac{\rho_0}{(r/R)(1 + r/R)^2}, \tag{23}$$

where G_N is the Newton's constant, $R = 20$ kpc and we choose $\rho_0 = 0.34\ {\rm GeV/cm^3}$ such that near the Solar System $\rho(r_\odot) = 0.4\ {\rm GeV/cm^3}$. For the gamma ray observation by Fermi-LAT, the Ω integral covers the $15^\circ \times 15^\circ$ region around the Galactic center [19].

As discussed in the previous section, the annihilation of DM could happen in two ways:

$$\chi\bar{\chi} \to 2V, \quad \chi\bar{\chi} \to B \to nV \quad (n = 2, 3).$$

The first line is the usual direct annihilation with Sommerfeld enhancement, while the second line corresponds to having a bound state formation and then DM annihilating within the bound states. The number of dark photons resulting from this annihilation, $n = 2, 3$, depends on the C parity $C = (-1)^{\ell+S}$ of the bound state B that decays via DM annihilation. In Eq. (22), the function $dN_\gamma^{(n)}/dE_\gamma$ is the photon spectrum at the source, depending on the number of V's in the final state ($n = 2, 3$). We describe the details of our calculation of $dN_\gamma^{(n=2,3)}/dE_\gamma$ in Appendix A.

The cross sections for $n = 2$, 3 are related to the ones discussed in the previous section as

$$(\sigma v)_{2V} = (\sigma v)_{\rm A} + (\sigma v)_{\rm B} f_2, \tag{24}$$

$$(\sigma v)_{3V} = (\sigma v)_{\rm B} (1 - f_2). \tag{25}$$

The factor f_2 is the fraction of bound states annihilating into $2V$ from the state with $C = +1$. The rest of the bound states will annihilate to $3V$ with $C = -1$. As shown by Fig. 5, we find the $3V$ channel yields only a slightly larger (and slightly softer) gamma ray flux than the $2V$ channel. Thus our numerical results are insensitive to the value of f_2. For convenience, we use $f_2 = 1$ in the following calculations, which yields the most conservative limits.

In general, one has to calculate the cross section $(\sigma v)_{nV}$ within the line of sight integral because the bound state formation cross section is velocity dependent, as discussed in Fig. 3, and the DM velocity near the Galactic center depends on the position r. For simplicity, we neglect the r dependence and assume Maxwell-Boltzmann velocity distribution of DM with a reasonable root-mean-square value $v_{\rm rms} = 150$ km/s throughout the signal region at the Galactic center as suggested in [20]. This approximation does not affect the main point of our work.

We compare the gamma ray spectrum with the one from the Galactic center observed by Fermi-LAT [19]. We find that for the multi-TeV DM in this study, the resulting

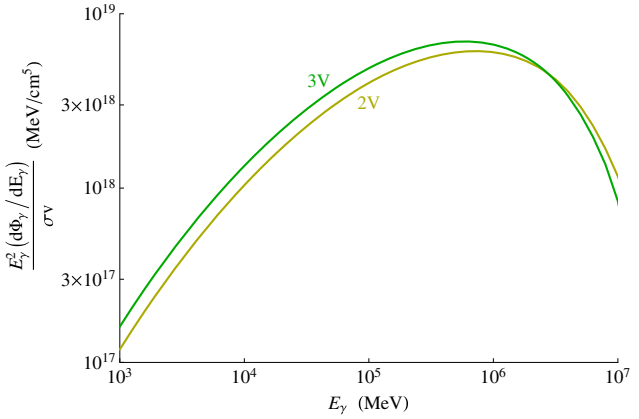

FIG. 5. An example of gamma ray fluxes per unit cross section as a function of photon energy for the $2V$ and $3V$ channels. Here the dark matter is $m_D = 16.7$ TeV and dark photon mass is $m_D = 10$ GeV.

gamma ray spectrum is peaked around a few hundred GeV to a TeV, while in the Fermi data, a spectrum decreasing with energy is provided only in the window 1–100 GeV. Therefore, the last bin with $E_\gamma \sim 80$ GeV provides the strongest upper limit. As discussed above, we assume that all DM bound states annihilate decay into $2V$. The relevant cross section is just

$$(\sigma v)_{2V} = (\sigma v)_{\rm A} + (\sigma v)_{\rm B}. \tag{26}$$

This quantity as a function of m_V is shown in Fig. 6, for $m_D = 16.7$ TeV, $\alpha_D = 0.2$. For m_V less than the typical DM momentum at the Galactic center, $(\sigma v)_{2V}$ has similar dependence on m_V as Fig. 2, because the DM annihilation

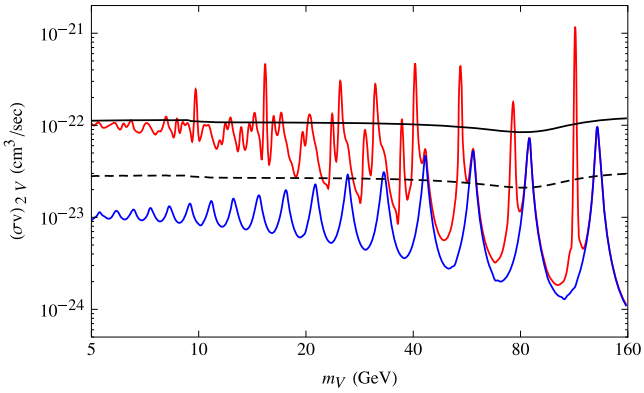

FIG. 6. Cross section for dark matter annihilation for indirect detection of gamma rays. We take $m_D = 16.7$ TeV and $\alpha_D = 0.2$. The effect of dark matter bound states is included in the red curve [we choose $f_2 = 1$, see Eqs. (24) and (25)] but not the blue one. The horizontal black curves correspond to the most conservative upper limit without including any interstellar emission background models (solid curve), and the upper limit with background included (dashed curve). Including the dark matter bound state formations results in a much stronger bound.

via bound state formation gives the dominant effect for indirect detection. In contrast, we also show the direct annihilation cross section with Sommerfeld enhancement (often considered in the literature) in the blue curve, which can be lower than the total effective cross section by an order of magnitude. The solid black curve is the most conservative upper limit on $(\sigma v)_{\rm eff}$ by assuming zero background and requiring the signal from annihilation itself does not exceed the Fermi observation. The dashed black curve corresponds to taking into account the background using the interstellar emission models discussed in [19], which sets a more stringent upper limit than the conservative one by a factor of ∼4. Clearly, the effect of bound state formation at the Galactic center can make a large difference. Given the other parameters, the upper limit on the dashed curve already rules out the region $m_V < 20$ GeV, while it would still be allowed if we only considered the direct annihilation channel with Sommerfeld enhancement.

In Fig. 7, we show the impact of bound state formation on indirect detection in the m_V versus m_D parameter space plane. The value of α_D is chosen to give the correct thermal relic density for DM (see also the discussion in the next section). In the plot on the left, we calculate the DM direct annihilation cross section with Sommerfeld enhancement and show the Fermi gamma ray constraint including the astrophysical background. The green region is excluded. In the plot on the right, we include the effect from DM bound state formation and the magenta region is further ruled out. Clearly, bound state effects can play a very important role and must be included for DM masses above a few TeV. In particular, for the window $m_V \in (1-10)$ GeV, thermal DM with $m_D \gtrsim 8$ TeV is allowed by the Fermi gamma ray data if we only consider the Sommerfeld enhanced direct annihilation. However, if we take into account of the contribution from the annihilation via bound state formation, the region of allowed DM mass increases to $m_D > 30$ TeV.

IV. THERMAL RELIC DENSITY

In this section, we discuss the impact of bound state formation on DM thermal freeze-out. As shown in Fig. 3, around the freeze-out temperature when the DM velocity is $v \sim 0.3$, the bound state formation cross section is comparable to the direct annihilation one. One might think this would modify the effective annihilation cross section and in turn the value of α_D that gives rise to the observed thermal relic DM density.

However, there is another important process which is bound state dissociation. Because the Universe is hot during the time of freeze-out, there is a plasma of the mediator V particles around. For the part of the parameter space where bound states exist, the freeze-out temperature T_f is much larger than m_V. The dissociation process happens when an energetic V particle collides with a bound state and breaks it into free χ and $\bar{\chi}$ particles. Because $\alpha_D/v \sim 1$ during

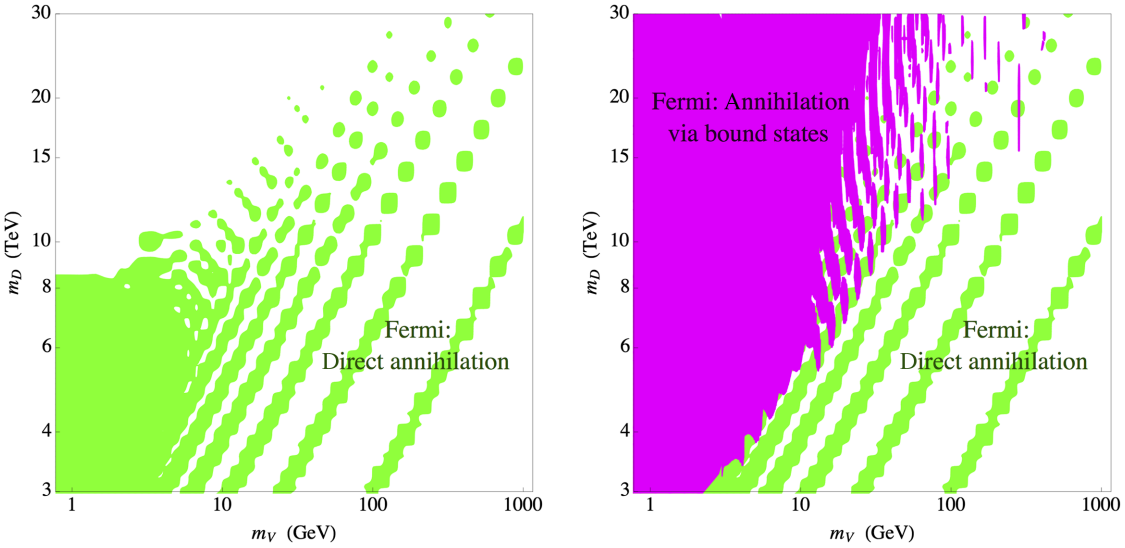

FIG. 7. The importance of dark matter bound states for constraining the parameter space of the dark matter–dark photon model. Here we zoom in to the region of parameter space marked by "Focus of this study" in Fig. 1 in the $m_V - m_D$ plane. The green region shows the exclusion from indirect detection of gamma ray and includes only dark matter direct annihilation from the Galactic center. The magenta region in the plot on the right shows the (stronger) constraint when dark matter bound state formation effect is taken into account.

freeze-out, capture into the first few bound state energy levels dominates. We will use the $S = 0$ ground state to compare the dissociation and decay rates.[3]

The decay rate of the ground state, which we call η_D, is approximately

$$\Gamma(\eta_D \to 2V) = \frac{1}{2}\alpha_D^5 m_D, \tag{27}$$

where we neglect the impact of the η_D binding energy on the mass of η_D.

The dissociation rate of η_D is

$$\Gamma(V\eta_D \to \chi\bar{\chi}) = \left[\frac{3\zeta[3]}{\pi^2}T_f^3\right]\left[\frac{8\sqrt{3}}{9}\left(\frac{m_D}{T_f}\right)^3\right] \times \left[\frac{128\pi\alpha_D^5}{9T_f^{1/2}m_D^{3/2}(\alpha_D^2 + 3T_f/m_D)}\right], \tag{28}$$

where the first factor is the number density of V particles, the second factor is the ratio of the bound state dissociation cross section to the formation one obtained in [21] (which applies for both vector and scalar mediator cases), and the last factor is the bound state formation cross section equation (12) for $n = 1$. We have also used the condition $v \simeq \sqrt{3T_f/m_D}$ and the approximation $T_f \ll m_D$.

Using the usual thermal value of α_D that gives the DM relic density, and the typical freeze-out temperature $T_f \sim m_D/30$, we find the ratio

$$\frac{\Gamma(V\eta_D \to \chi\bar{\chi})}{\Gamma(\eta_D \to 2V)} > 10, \tag{29}$$

for all the parameter space where $\alpha_D < 0.3$. Therefore, the DM bound state is quickly dissociated by a collision with a V before it has enough time to decay by DM-anti-DM annihilation. After the dark matter annihilates down to its relic density bound states are rapidly dissociated by the scattering process which has a rate with one less factor of the dark number density than the bound state formation process. This dissociation rate is much larger than the Hubble rate at this time and so is effective at removing the bound states. On the other hand, the formation of bound states which involves two factors of the dark matter number density occurs at a rate less than the Hubble rate and so is ineffective. We conclude that bound state formation is unimportant during the thermal freeze-out of DM.

V. CMB

Dark matter annihilation during recombination injects energy in the Universe and could distort the CMB spectrum. In this era, the DM velocity is very low, $v \sim 10^{-10} \ll m_V/m_D$ and α_D. One cannot take a very tiny dark photon mass to violate this condition, otherwise it would cause too strong DM self-interactions and run into conflict with the bullet cluster observation [22]. We find that the bound state formation only involves the transition from s-wave scattering state to p-wave bound states, and its cross section is much lower than the direct annihilation one with the Sommerfeld enhancement (see Fig. 3). Thus the usual constraint from CMB still applies [23–25]. For such low velocity, we use an approximate Sommerfeld factor S

[3]The $s = 1$ state decays into $3V$ at a slower rate, and the $n > 1$ bound states are shallower and easier to be dissociated.

obtained from the Hulthén potential [26,27], which is bounded from below, $S \geq 6\alpha_D m_D/m_V$. We presented the CMB excluded region of parameter space in yellow in Fig. 1.

VI. SUMMARY AND DISCUSSION

One of the simplest and most studied models of dark matter is a SM singlet Dirac fermion that annihilates down to its relic density through its coupling to a massive dark photon. We have shown that for dark matter mass in the tens of TeV range and dark photon mass in the GeV range, indirect detection constraints for dark matter in our Galaxy are highly impacted by annihilation through dark matter–anti-dark matter bound states. In the regions where bound state formation is most important, annihilation through all possible bound states must be taken into account. In this work, we derived the general cross section for bound state formation with the radiation of a dark photon, and explored its dependence in the dark matter velocity and the dark photon mass. Our most important results are illustrated by Fig. 7 where the magenta region shows the additional parameter space ruled out when annihilation through bound states is taken into account. The effects are strongest for large α_D and when the dark photon mass is smaller than the typical momentum of dark matter in the Galaxy. We have also argued that bound state effects are not important for dark matter annihilation during freeze-out and recombination.

For dark matter indirect detection, we have only discussed the Fermi gamma ray constraint. Our goal in this paper is to point out the importance of bound state formation rather than providing a comprehensive list of all the constraints. The bound state effects are expected to be generic, and a more complete analysis of the bound state effects on indirect detection via various cosmic ray components will be published elsewhere [28].

Our results so far are based on the dark matter bound state formation cross section taking into account the emission of a single dark photon. In the limit of $m_V \to 0$, this cross section section is given by the Kramers formula in Eq. (11). Its ratio to the s-wave geometric cross section $\sigma_G = 4\pi/k^2$ is

$$\frac{\sigma_{\rm B}}{\sigma_G} \sim \alpha_D^3 \log\left(\frac{\alpha_D}{v}\right). \tag{30}$$

For the parameters of interest in this paper $\sigma_{\rm B}/\sigma_G \ll 1$, the unitarity bound is satisfied and hence we expect perturbation theory to be valid.

Finally, we comment on the case when the light mediator is a real scalar instead of a dark photon, which has also been considered in the literature. As pointed out in [21], because the operator for radiating a scalar is the unit operator and the scattering and bound state wave functions are orthogonal, the leading order matrix element arises from second order in the multiple expansion. As a result, the bound state formation cross section would go as α_D^5, in contrast to the α_D^3 for the dark photon model. Thus, the effects of bound state formation on dark matter indirect detection is weaker in the scalar model. It is worth mentioning that the scalar force is also attractive for same sign χ's and could result in bound states with a large number of DM particles that are stable, and may be cosmological important in the asymmetric dark matter case [29].

ACKNOWLEDGMENTS

We thank Clifford Cheung, Walter D. Goldberger and Maxim Pospelov for the useful discussions. This work is supported by U.S. DOE Grants No. DE-SC0011632, and No. DE-SC0010255, and by the Gordon and Betty Moore Foundation through Grant No. 776 to the Caltech Moore Center for Theoretical Cosmology and Physics. We are also grateful for the support provided by the Walter Burke Institute for Theoretical Physics. H. A. acknowledges the hospitality from the Perimeter Institute for Theoretical Physics.

APPENDIX A: PROMPT PHOTON SPECTRUM

For V heavier than a few GeV perturbative methods for calculating V decaying to quarks are applicable. We extrapolate those results into the region of lighter V, much of which is already strongly constrained by the CMB, see Fig. 1. The prompt photons from the products of V decay dominate the source term $dN_\gamma^{(n)}/dE_\gamma$ at large photon energy E_γ, and results in a peak in the spectrum. Other contributions to gamma ray from bremsstrahlung and inverse Compton scattering by charged particles (electrons) in the final states are only important for photon energies much lower than the peak energy [30]. We first calculate the energy spectrum of V from dark matter annihilations. Because the dark matter is nonrelativistic in the Galaxy, the energy distribution of a $2V$ final state per reaction is always

$$\frac{dN_V^{(2)}}{dy}(y) = 2\delta(y-1), \tag{A1}$$

where $y = E_V/m_D$. On the other hand, for the $3V$ final state, the distribution is (for $m_V \ll m_D$) [31]

$$\frac{dN_V^{(3)}}{dy}(y) = \frac{9}{4(\pi^2-9)y^2}\left[y(3y-8) + \frac{(y-1)(y^2-6y+16)\ln(1-y)}{y-2}\right] \times \left(\frac{1}{1-m_V/m_D-3m_V^2/(4m_D^2)}\right), \tag{A2}$$

and in this case y is between $y_{\min} = m_V/m_D$, $y_{\max} = 1 - 3m_V^2/(4m_D^2)$. The V's will subsequently decay into charged fermion pairs f, $\bar{f}$. It is easy to show that the energy distribution of f in the boosted V frame is flat,

$$\frac{dN_f}{dE_f}(y) \simeq \frac{2}{y m_D \sqrt{1-\frac{4m_f^2}{m_V^2}}},$$
$$(E_f)^{\max}_{\min}(y) = \frac{1}{2} y m_D \left(1 \pm \sqrt{1-\frac{4m_f^2}{m_V^2}}\right). \quad \text{(A3)}$$

Here we have used the approximation that for $m_D \gg m_V$, in most of the final state phase space $E_V = y m_D \gg m_V$. Therefore, the photon energy spectrum (prompt, from final state radiation) per annihilation is given by

$$\frac{dN_\gamma^{(n,f)}}{dE_\gamma} = \int_{y_{\min}}^{y_{\max}} dy \frac{dN_V^{(n)}}{dy}(y) \times \int_{(E_f)_{\min}(y)}^{(E_f)_{\max}(y)} dE_f \frac{dN_f}{dE_f}(y) \frac{dN_\gamma^0}{dE_\gamma}(E_f, E_\gamma/E_f), \quad \text{(A4)}$$

where dN_γ^0/dE_γ is the photon distribution function per each injection of a DM charged particle f, and is obtained using the code PPPC4 [32]. Finally, the total photon energy spectrum is obtained by summing over the possible fermion flavors f, weighed by the branching ratio of the decay $V \to f\bar{f}$,

$$\frac{dN_\gamma^{(n)}}{dE_\gamma} = \sum_f \frac{dN_\gamma^{(n,f)}}{dE_\gamma} \mathrm{Br}(V \to f\bar{f}). \quad \text{(A5)}$$

We give the decay rates for $V \to f\bar{f}$ in Appendix B.

For the $3V$ channel ($n = 3$) Eq. (A5) can be simplified by interchanging orders of integration. After some algebra,

$$\frac{dN_\gamma^{(3,f)}}{dE_\gamma} = \int_{(E_f)_{\min}(y_{\min})}^{(E_f)_{\max}(y_{\max})} dE_f \frac{1}{m_D}[F(y_+) - F(y_-)] \times \frac{dN_\gamma}{dE_\gamma}(E_f, E_\gamma/E_f), \quad \text{(A6)}$$

where

$$F(y) = \frac{-9[4y + \ln(1-y)(4 - 7y + 3y^2 - y^2\ln(2-y)) - y^2 \mathrm{PolyLog}(2, y-1)]}{2y^2(\pi^2 - 9)(1 - m_V/m_D - 3m_V^2/(4m_D^2))\sqrt{1 - 4m_f^2/m_V^2}}, \quad \text{(A7)}$$

and

$$y_+ = \mathrm{Min}\left[1 - \frac{3m_V^2}{4m_D^2}, \frac{2E_f/m_D}{1-\sqrt{1-\frac{4m_f^2}{m_V^2}}}\right],$$
$$y_- = \mathrm{Max}\left[\frac{m_V}{m_D}, \frac{2E_f/m_D}{1+\sqrt{1-\frac{4m_f^2}{m_V^2}}}\right]. \quad \text{(A8)}$$

APPENDIX B: DARK PHOTON DECAY RATES

In general, the kinetic mixing between the dark photon and the usual photon originates from the $SU(2) \times U(1)$ gauge invariant operator $\frac{\kappa}{2\cos\theta_w} B_{\mu\nu} V^{\mu\nu}$, where B_μ is the gauge field for hypercharge. After the electroweak symmetry breaking, this operator not only induces the kinetic mixing term $\frac{\kappa}{2} F_{\mu\nu} V^{\mu\nu}$ in Eq. (1), but also a kinetic mixing between V and the Z boson, $-\frac{\kappa \tan\theta_w}{2} Z_{\mu\nu} V^{\mu\nu}$. Therefore, the branching ratios of V is not simply like those of a massive photon. The kinetic mixing between V and Z can play an important role for $m_V \gg$ GeV.

The Feynman diagrams for V decaying to fermion pairs via the off-shell photon and the Z boson are shown in Fig. 8. The effective coupling of an on-shell V to the left- (right-) handed fermion current is

$$g_L = \kappa g \sin\theta_w \left[Q_f - \frac{m_V^2}{m_V^2 - m_Z^2} \frac{1}{\cos^2\theta_w}(T_3^f - Q_f \sin^2\theta_w)\right],$$
$$g_R = \kappa g \sin\theta_w \left[Q_f - \frac{m_V^2}{m_V^2 - m_Z^2} \frac{1}{\cos^2\theta_w}(-Q_f \sin^2\theta_w)\right]. \quad \text{(B1)}$$

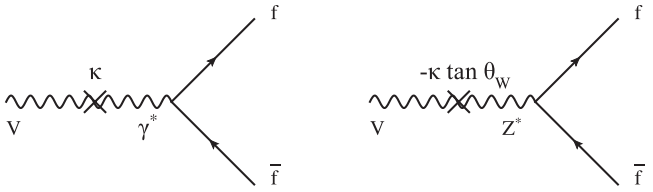

FIG. 8. Feynman diagrams for the dark photon V decaying to fermions, via an off-shell photon or the Z boson.

The decay rates are then [33]

$$\Gamma_{V\to f\bar{f}} = \frac{N_c^f m_V}{24\pi}(1-4r_f)^{1/2}[g_L^2(2-2r_f) + g_R^2(2-2r_f) - 12 g_L g_R r_f], \quad \text{(B2)}$$

where $r_f = m_f^2/m_V^2$, and $N_c^f = 3$ for quarks and 1 for charged leptons and neutrinos. For the parameter space of interest to this study, m_V lies between ~GeV and the weak scale. We obtain the total decay rate by summing over all possible quark and lepton flavors that are kinematically allowed for V to decay into.

[1] H. A. Kramers, On the theory of X-ray absorption and of the continuous X-ray spectrum, Philos. Mag. **46**, 836 (1923).
[2] V. M. Katkov and V. M. Strakhovenko, Radiative recombination and its application in experiments on electron cooling, J. Exp. Theor. Phys. **48**, 4 (1978).
[3] H. A. Bethe and E. E. Salpeter, *Quantum Mechanics of One- and Two-Electron Atoms* (Springer-Verlag, New York, 1957).
[4] M. Pospelov and A. Ritz, Astrophysical signatures of secluded dark matter, Phys. Lett. B **671**, 391 (2009).
[5] J. D. March-Russell and S. M. West, WIMPonium and boost factors for indirect dark matter detection, Phys. Lett. B **676**, 133 (2009).
[6] L. Pearce, K. Petraki, and A. Kusenko, Signals from dark atom formation in halos, Phys. Rev. D **91**, 083532 (2015).
[7] K. Petraki, M. Postma, and M. Wiechers, Dark-matter bound states from Feynman diagrams, J. High Energy Phys. 06 (2015) 128.
[8] J. L. Feng, M. Kaplinghat, H. Tu, and H. B. Yu, Hidden charged dark matter, J. Cosmol. Astropart. Phys. 07 (2009) 004.
[9] B. von Harling and K. Petraki, Bound-state formation for thermal relic dark matter and unitarity, J. Cosmol. Astropart. Phys. 12 (2014) 033.
[10] M. Cirelli, M. Kadastik, M. Raidal, and A. Strumia, Model-independent implications of the e^{+-}, anti-proton cosmic ray spectra on properties of dark matter, Nucl. Phys. **B813**, 1 (2009); **B873**, 530 (2013).
[11] N. Arkani-Hamed, D. P. Finkbeiner, T. R. Slatyer, and N. Weiner, A theory of dark matter, Phys. Rev. D **79**, 015014 (2009).
[12] P. J. Fox and E. Poppitz, Leptophilic dark matter, Phys. Rev. D **79**, 083528 (2009).
[13] D. S. Akerib *et al.* (LUX Collaboration), Improved Limits on Scattering of Weakly Interacting Massive Particles from Reanalysis of 2013 LUX data, Phys. Rev. Lett. **116**, 161301 (2016).
[14] J. D. Bjorken, R. Essig, P. Schuster, and N. Toro, New fixed-target experiments to search for dark gauge forces, Phys. Rev. D **80**, 075018 (2009).
[15] J. B. Dent, F. Ferrer, and L. M. Krauss, Constraints on light hidden sector gauge bosons from supernova cooling, arXiv: 1201.2683.
[16] D. Kazanas, R. N. Mohapatra, S. Nussinov, V. L. Teplitz, and Y. Zhang, Supernova bounds on the dark photon using its electromagnetic decay, Nucl. Phys. **B890**, 17 (2014).
[17] Y. Zhang, Long-lived light mediator to dark matter and primordial small scale spectrum, J. Cosmol. Astropart. Phys. 05 (2015) 008.
[18] M. Kaplinghat, S. Tulin, and H. B. Yu, Direct detection portals for self-interacting dark matter, Phys. Rev. D **89**, 035009 (2014).
[19] M. Ajello *et al.* (Fermi-LAT Collaboration), Fermi-LAT observations of high-energy gamma-ray emission toward the Galactic center, Astrophys. J. **819**, 44 (2016).
[20] D. P. Finkbeiner, L. Goodenough, T. R. Slatyer, M. Vogelsberger, and N. Weiner, Consistent scenarios for cosmic-ray excesses from Sommerfeld-enhanced dark matter annihilation, J. Cosmol. Astropart. Phys. 05 (2011) 002.
[21] M. B. Wise and Y. Zhang, Stable bound states of asymmetric dark matter, Phys. Rev. D **90**, 055030 (2014); **91**, 039907(E) (2015).
[22] S. W. Randall, M. Markevitch, D. Clowe, A. H. Gonzalez, and M. Bradac, Constraints on the self-interaction cross-section of dark matter from numerical simulations of the merging galaxy cluster 1E 0657-56, Astrophys. J. **679**, 1173 (2008).
[23] S. Galli, F. Iocco, G. Bertone, and A. Melchiorri, CMB constraints on dark matter models with large annihilation cross-section, Phys. Rev. D **80**, 023505 (2009).
[24] T. R. Slatyer, N. Padmanabhan, and D. P. Finkbeiner, CMB constraints on WIMP annihilation: Energy absorption during the recombination epoch, Phys. Rev. D **80**, 043526 (2009).
[25] T. R. Slatyer, Indirect dark matter signatures in the cosmic dark ages. I. Generalizing the bound on s-wave dark matter annihilation from Planck results, Phys. Rev. D **93**, 023527 (2016).
[26] S. Cassel, Sommerfeld factor for arbitrary partial wave processes, J. Phys. G **37**, 105009 (2010).
[27] J. L. Feng, M. Kaplinghat, and H. B. Yu, Sommerfeld enhancements for thermal relic dark matter, Phys. Rev. D **82**, 083525 (2010).
[28] H. An and Y. Zhang (to be published).
[29] M. B. Wise and Y. Zhang, Yukawa bound states of a large number of fermions, J. High Energy Phys. 02 (2015) 023; 10 (2015) 165(E).

[30] P. Meade, M. Papucci, A. Strumia, and T. Volansky, Dark matter interpretations of the e^{+-} excesses after FERMI, Nucl. Phys. **B831**, 178 (2010).

[31] H. An, B. Echenard, M. Pospelov, and Y. Zhang, Probing the Dark Sector with Dark Matter Bound States, Phys. Rev. Lett. **116**, 151801 (2016).

[32] M. Cirelli *et al.*, PPPC4 DM ID: A poor particle physicist cookbook for dark matter indirect detection, J. Cosmol. Astropart. Phys. 03 (2011) 051; 10 (2012) E01.

[33] D. Curtin, R. Essig, S. Gori, and J. Shelton, Illuminating dark photons with high-energy colliders, J. High Energy Phys. 02 (2015) 157.